Computer Methods and Programs in Biomedicine 252 (2024) 108215

Contents lists available at ScienceDirect

Computer Methods and Programs in Biomedicine

journal homepage: https://www.sciencedirect.com/journal/computer-methods-and-programs-in-biomedicine

Cyto R-CNN and CytoNuke Dataset: Towards reliable whole-cell segmentation in bright-field histological images

Johannes Raufeisen [a,b,c], Kunpeng Xie [a,b,c], Fabian Hörst [d,e], Till Braunschweig [g,c,h], Jianning Li [d,e], Jens Kleesiek [d,e,f], Rainer Röhrig [b,c], Jan Egger [d,e,i], Bastian Leibe [j], Frank Hölzle [a,c], Alexander Hermans [j], Behrus Puladi [a,b,c,*]

[a] Department of Oral and Maxillofacial Surgery, University Hospital RWTH Aachen, Pauwelsstr. 30, 52074 Aachen, Germany
[b] Institute of Medical Informatics, University Hospital RWTH Aachen, Pauwelsstr. 30, 52074 Aachen, Germany
[c] Center for Integrated Oncology Aachen Bonn Cologne Düsseldorf (CIO ABCD), Pauwelsstraße 30, 52074 Aachen, Germany
[d] Institute for Artificial Intelligence in Medicine (IKIM), University Hospital Essen (AöR), Girardetstraße 2, 45131 Essen, Germany
[e] Cancer Research Center Cologne Essen (CCCE), West German Cancer Center Essen, University Hospital Essen (AöR), Hufelandstr. 55, 45147 Essen, Germany
[f] Department of Physics, TU Dortmund University, August-Schmidt-Str. 4, 44227 Dortmund, Germany
[g] Institute of Pathology, University Hospital RWTH Aachen, Pauwelsstr. 30, 52074 Aachen, Germany
[h] Institute of Pathology, LMU Munich, Thalkirchner Str. 36, 80337 Munich, Germany
[i] Center for Virtual and Extended Reality in Medicine (ZvRM), University Hospital Essen, University Medicine Essen, Hufelandstraße 55, 45147 Essen, Germany
[j] Visual Computing Institute (Computer Vision), RWTH Aachen University, Mies-van-der-Rohe Str. 15, 52074 Aachen, Germany

ARTICLE INFO

Dataset link: https://doi.org/10.5281/zenodo.10560728

MSC:
68T07
68T45

Keywords:
Digital pathology
Cell segmentation
Deep learning

ABSTRACT

Background and objective: Cell segmentation in bright-field histological slides is a crucial topic in medical image analysis. Having access to accurate segmentation allows researchers to examine the relationship between cellular morphology and clinical observations. Unfortunately, most segmentation methods known today are limited to nuclei and cannot segment the cytoplasm.

Methods: We present a new network architecture Cyto R-CNN that is able to accurately segment whole cells (with both the nucleus and the cytoplasm) in bright-field images. We also present a new dataset CytoNuke, consisting of multiple thousand manual annotations of head and neck squamous cell carcinoma cells. Utilizing this dataset, we compared the performance of Cyto R-CNN to other popular cell segmentation algorithms, including QuPath's built-in algorithm, StarDist, Cellpose and a multi-scale Attention Deeplabv3+. To evaluate segmentation performance, we calculated AP50, AP75 and measured 17 morphological and staining-related features for all detected cells. We compared these measurements to the gold standard of manual segmentation using the Kolmogorov–Smirnov test.

Results: Cyto R-CNN achieved an AP50 of 58.65% and an AP75 of 11.56% in whole-cell segmentation, outperforming all other methods (QuPath 19.46/0.91%; StarDist 45.33/2.32%; Cellpose 31.85/5.61%, Deeplabv3+ 3.97/1.01%). Cell features derived from Cyto R-CNN showed the best agreement to the gold standard ($\overline{D} = 0.15$) outperforming QuPath ($\overline{D} = 0.22$), StarDist ($\overline{D} = 0.25$), Cellpose ($\overline{D} = 0.23$) and Deeplabv3+ ($\overline{D} = 0.33$).

Conclusion: Our newly proposed Cyto R-CNN architecture outperforms current algorithms in whole-cell segmentation while providing more reliable cell measurements than any other model. This could improve digital pathology workflows, potentially leading to improved diagnosis. Moreover, our published dataset can be used to develop further models in the future.

1. Introduction

Advances in artificial intelligence (AI) and digital pathology have revolutionized medical research. Nowadays, it is possible to extract precise information about a tumor just from its microscopical image. For example, neural networks have made it possible to predict a tumor's malignancy and prognosis [1] and can even detect genetic differences just from histological images [2]. These advancements are particularly valuable, because they are able to operate on hematoxylin-eosin (HE) stained images. This is a great achievement, because HE staining is inexpensive, widespread and part of many clinical routines [3].

* Correspondence to: Department of Oral and Maxillofacial Surgery and Institute of Medical Informatics, University Hospital RWTH Aachen, Pauwelsstr. 30, 52074 Aachen, Germany
E-mail address: bpuladi@ukaachen.de (B. Puladi).

https://doi.org/10.1016/j.cmpb.2024.108215
Received 6 February 2024; Received in revised form 19 April 2024; Accepted 6 May 2024
Available online 11 May 2024

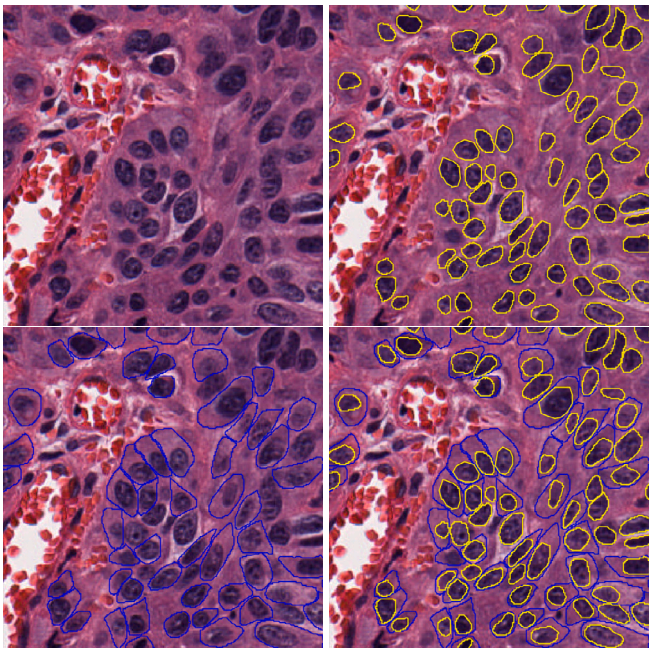

Fig. 1. A sample image from the CytoNuke dataset. Tumor nuclei annotations are shown in yellow, tumor cell annotations are shown in blue. Not every nucleus annotation has a corresponding cell annotation, since cell boundaries are not always clearly distinguishable. In such cases, only the cell's nucleus was annotated.

However, understanding the reasoning of these neural networks is not always straightforward. This is why explainability is such an important factor, both for research purposes as well as for bringing AI into clinical routine [4]. As shown by Diao et al. [5] automated cell segmentation can help fill that gap in explainability, because the cell nucleus and cytoplasm contains important morphological and staining-related information. If this information can be automatically extracted from histological images via cell segmentation, this can potentially offer explanations for the predictions of a neural network.

For this reason, we developed a cell segmentation algorithm that can segment both the nucleus and the cytoplasm in HE-stained histological images. We conducted a number of experiments to compare our method against QuPath, StarDist, Cellpose and the gold standard of manual segmentation.

1.1. Related work

Whole cell segmentation is a well-studied topic in cytology and immunofluorescence imaging. Over the last years, multiple algorithms have been developed to support both nucleus and cytoplasm segmentation in different cytological image modalities [6]. Most recently, the SegPC-2021 challenge [7], inspired multiple solutions for whole cell segmentation of multiple myeloma cells.

Unfortunately, methods coming from the cytological domain are often unsuitable for histological bright-field images, in particular when dealing with hematoxylin-eosin (HE) staining. This is due to a few key differences between cytological and histological images. First, cytological images usually have a uniform background and contain only fewer, separated cells. In histological images, the opposite is true. There is barely any background visible and the whole image is filled with contiguous cells. Second, in cytological images cell usually has a clearly distinguishable cell membrane. This is not the case for all histological images. In HE-stained tissue slides, the cells are so close together that it is not possible to identify the cell membrane in all cases.

For these reasons, algorithms developed for whole cell segmentation in cytology often cannot be directly applied to HE-stained histology. For example, the winning submission of the SegPC-2021 challenge leverages a "'whole-cell' class to help predictions of the two classes of interest, namely nucleus and cytoplasm" [7]. This assumption does not hold for all cells in histological HE-stained images.

Therefore, most histopathological papers use a different method for cellular analysis in bright-field images. In a first step, the nucleus is segmented, e.g. via QuPath [8] or StarDist [9]. In a second step, the heuristic of "cell expansion" is used. This heuristic will approximate the cell boundary and thus offer a whole-cell and cytoplasm segmentation mask. This method can be considered state-of-the-art in histopathological analysis. It is implemented in standard pathological software such as QuPath and CellProfiler [10] and is used across several impactful papers [11–14].

Despite its popularity, it can be shown that cell expansion does not always perform well on bright-field histological images. Under some circumstances it is possible that cell expansion provides very unreliable segmentations. These segmentations will then result in inaccurate measurements of morphological and staining-related properties.

In this paper, we will develop a method for whole cell segmentation that can deal well with the peculiarities of HE-stained histological images and offer more reliable measurements than the state-of-the-art cell expansion.

2. Material and methods

We developed a new architecture based on Mask R-CNN for whole-cell segmentation in hematoxylin-eosin stained bright-field histological images. We then compared this architecture against cell segmentation algorithms from StarDist, Cellpose and QuPath. To enable a fair comparison, all methods needed to be evaluated on the same dataset. To the authors' knowledge, there is no publicly available dataset that contains both nucleus and cytoplasm annotations in HE images. For this reason, we created a new dataset which is being published alongside this paper. Using this new dataset, the models have been evaluated under different categories. First, the segmentation accuracy has been compared using the standard measures AP50 and AP75. In a second step, the predicted cell segmentations were imported into QuPath to measure a number of cell features. These cell features were then statistically compared against the gold standard measurements.

2.1. Dataset

We created a dataset of nuclei and cell annotations using publicly available images of head and neck squamous cell carcinoma (HNSCC) from the CPTAC dataset [15,16]. Nuclei and cells were manually annotated in QuPath (version 0.4.3) by J.R. and K.X. All annotations were reviewed by a third investigator B.P. and finally reviewed and approved by a senior pathologist T.B. The resulting annotations were then exported from QuPath as COCO-compatible JSON files. The corresponding images were exported in patches of 256×256 px at a resolution of 0.5 μm/px.

As the CPTAC dataset contains whole slide images from multiple facilities, the staining intensities can vary between images. To eliminate these differences, all images were normalized using the Macenko algorithm [17]. This is a standard practice used to facilitate training of deep learning models [18]. The resulting images were then split into a training (70%), validation (15%) and test set (15%) To avoid overfitting, we made sure not to allocate images from the same patient to different subsets.

The resulting dataset contains 3991 tumor nuclei and 2607 tumor cell annotations. Fig. 1 shows an example image from our dataset with corresponding annotations.

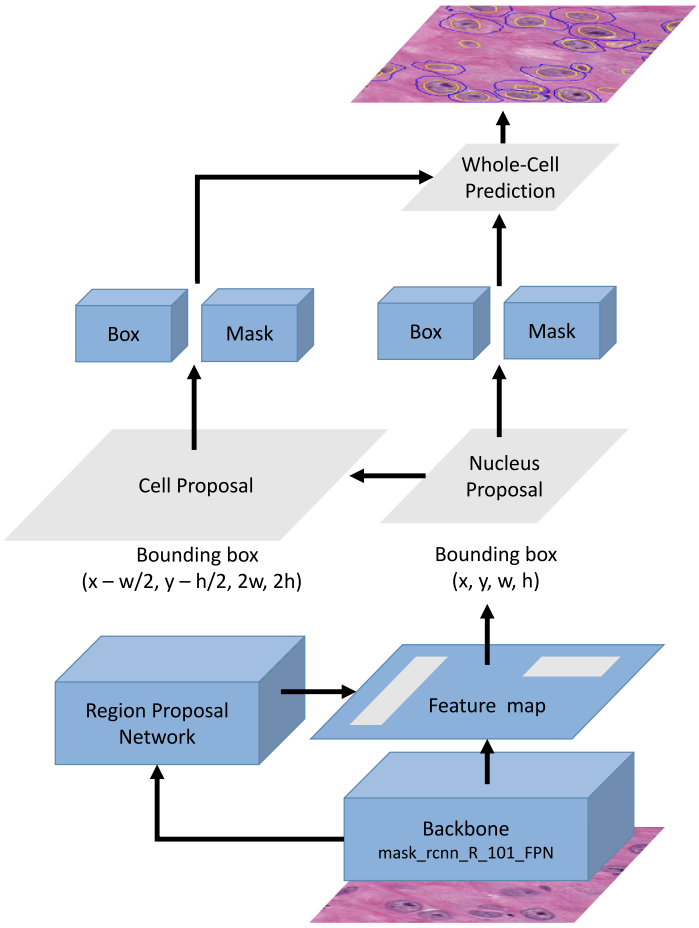

Fig. 2. Architectural overview of Cyto R-CNN. The backbone and region proposal network (RPN) are trained to only predict nuclei. The nuclei proposals are then forwarded to two different branches. The first branch will perform a regular bounding box and mask regression for the nucleus. The second branch will scale the nucleus proposal and perform mask regression for the whole cell, including the cytoplasm. Both branches are then combined to generate instance segmentations for cell and nucleus at the same time.

2.2. Methods

2.2.1. QuPath

QuPath is a popular software tool to analyze whole slide images and is widely used in pathological research [8,19]. It provides a built-in cell and nuclei segmentation algorithm, which we used as a baseline for our experiments.

The nucleus detection within QuPath is built upon the watershed algorithm, which utilizes the fact that a nucleus appears darker than its surrounding cytoplasm when stained by HE. To detect the whole cell including its cytoplasm, QuPath implements a method known as "nucleus expansion" [20] or "cell expansion" [14]. This algorithm will expand each nucleus by a fixed number of pixels as long as the expansion does not intersect with the expansion of an adjacent nucleus.

Since the watershed algorithm is sensitive to its hyperparameters, QuPath has been evaluated in two different modes: Once with default settings and once with a set of improved parameters.

The default settings in QuPath version 0.4.3 were as follows: A background radius of 8 µm, a sigma of 1.5 µm, a minimum area of 10 μm^2, a maximum area of 400 μm^2, an intensity threshold of 0.1 and a cell expansion radius of 5 µm. We heuristically tuned the parameters on our validation dataset and found the following values to deliver good results for nucleus segmentation on our dataset: A sigma of 2.5 µm, a minimum area of 20 μm^2, a maximum area of 400 μm^2 and an intensity threshold of 0.15. The best expansion radius was identified to be 5 µm.

2.2.2. StarDist

StarDist is a U-Net based architecture developed specifically for the purpose of nucleus segmentation [9]. It is built on the assumption that a nucleus' shape can be approximated by a star-convex polygon. For each pixel, StarDist predicts both the object probability and the distance towards the boundary of the nucleus across 32 directions.

For our experiments, we experimented with both training the network from scratch as well as using the pre-trained model *2d_versatile_he*. Using the pre-trained model proved beneficial in our experiments. To avoid overfitting, the input data was augmented with random flips and rotations. After training, the best model was then combined with nucleus expansion. The best expansion radius was identified to be 5.5 µm.

2.2.3. Theoretical optimum of cell expansion

Cell expansion is a heuristic method that relies on an existing nucleus segmentation. We conduct another experiment to determine the theoretical optimum performance of cell expansion independently of the underlying nucleus segmentation. To achieve this, we use our ground-truth nucleus annotations and expand them with different radii. Under these conditions, the optimal expansion radius was identified to be 10 µm.

2.2.4. Cellpose

Cellpose is a second U-Net based architecture. Unlike StarDist however, Cellpose was originally designed to work with immunohistological images, where nucleus and cytoplasm were stained in high-contrast colors [21]. This special coloring allows Cellpose to perform color gradient tracking to derive the object masks. Since its invention, Cellpose has shown potential to generalize beyond its initial scope of immunofluorescence images [22].

We experimented with training Cellpose from scratch as well as finetuning it starting from a number of pre-trained models as published in Stringer and Pachitariu [23]. The input data was augmented with random flips and rotations. We also experimented with all possible combinations of color channels that serve as a hyperparameter for the Cellpose model.

Out of all the pre-trained Cellpose models, *CPx* performed best, both in nucleus and whole-cell segmentation. It delivered optimal performance when setting the nucleus channel to 3 and the cytoplasm channel to 0.

2.3. Multi-scale Attention Deeplabv3+

As part of the SegPC-2021 challenge, multiple methods for nucleus and cytoplasm segmentation in cytological images were developed. The two best-performing algorithms were an ensemble model presented by Faura et al. [24] and a multi-scale Attention Deeplabv3+ pipeline by Afshin et al. [25]. The first-place solution is not applicable to our dataset, as it requires each nucleus annotation to have a corresponding cytoplasm. The second place solution (Deeplabv3+) does not need this requirement, enabling us to include it in our experiments.

The Deeplabv3+ pipeline consists of multiple stages. In the first stage, a U-Net is trained for segmenting the nuclei. Afterwards, around each nucleus prediction multiple scaled image regions are extracted from the image. This extraction procedure is repeated for multiple scaling factors. Then, an Attention Deeplabv3+ model is trained for each scaling factor. Each model predicts the cytoplasm segmentation in a given image patch. In the final step, the different Deeplabv3+ models are combined. An aggregation function ensures that the optimal scaling factor is selected for each nucleus.

We include this method in our comparison to determine to what extent it is able to generalize from the cytological images in SegPC-2021 to the HE-stained images in our CytoNuke dataset. We experimented with training the nucleus and cytoplasm models from scratch as well as finetuning those models that were pretrained on the SegPC-2021 dataset. We found the performance to be slightly better when training the models from scratch.

2.3.1. Mask R-CNN

Mask R-CNN is a general-purpose instance segmentation architecture consisting of two stages [26]. The first stage extracts a number of rectangular regions of interest (ROIs) from the image. The second stage is responsible for classifying the object and predicting its binary object mask. This design has proven successful in many instance segmentation tasks, including nucleus segmentation [27,28].

However, a standard Mask R-CNN is unable to guarantee geometrical constraints between objects. In particular, nucleus and whole cell will be segmented independently from each other.

This will inevitably lead to suboptimal segmentation results. For example, it would be possible to predict a cytoplasm segmentation without a nucleus inside. Likewise, it would be possible that there are multiple cytoplasm segmentation masks for a single nucleus. From a medical and regulatory perspective, it is important to make these kinds of mistakes impossible by design.

2.4. Cyto R-CNN

Cyto R-CNN is a modified version of Mask R-CNN that encodes these geometrical constraints on an architectural level. Its design is illustrated in Fig. 2. The first stage is a standard regional proposal network, which is only trained on nucleus annotations. The second stage then splits into two branches: One for the nucleus and one for the whole cell. The nucleus branch consists of the regular Mask R-CNN steps: First a bounding box regression, then a binary mask prediction. The cell branch on the other hand has to first create a regional proposal for the cytoplasm. This is achieved by scaling the nucleus ROI by a fixed percentage. The resulting cell-ROI is then passed forward to a regular mask head. In a way, this modified region proposal network can be considered a deep-learning equivalent of the traditional cell expansion.

As Mask R-CNN is a large network, there are a number of hyperparameters that can be tuned. The backbone of Cyto R-CNN has been set to *mask_rcnn_R_101_FPN*, pre-trained on COCO [29] as provided by detectron. Training data was augmented with random flips and rotations. Different learning rates were evaluated using an exponential learning rate decay. Different cell scaling factors were evaluated as well. The optimal cell scaling factor for our dataset was determined to be 2.0. For the ROI heads, the non-maximum suppression was tuned due to the relatively large number of small objects in each image. A threshold of 0.3 delivered best results in our experiments.

2.5. Computational setup

Our experiments were performed on GPUs of type V100-SXM2. The algorithms were implemented using python 3.9, detectron2 [30], pytorch and tensorflow.

2.6. Statistical analysis

All methods were evaluated in their performance using class-specific AP50 and AP75. These two endpoints are commonly used in the literature [31,32], as they allow for insights not only into the detection accuracy, but also into the segmentation quality of a model. A model with high AP50, but low AP75 will be expected to detect objects quite well, but would fail to generate segmentation masks that accurately match their shape.

The segmentation masks produced by each model were subsequently imported into QuPath to measure a set of cell features related to morphology and staining. The features we chose for our comparison were: Cell area, perimeter, circularity, solidity, minimum and maximum diameter, cell-to-nucleus ratio, HE staining (median, mean, standard deviation, minimum, maximum). This specific set of features was chosen to resemble what is commonly used in the literature [12, 33–36].

The resulting measurements were then compared to the ground truth measurements using the Kolmogorov–Smirnov test. We used its test statistic D to quantify the similarity between the measurements derived from the different models and the measurements resulting from manual annotations. This statistical analysis was implemented in R (v4.2.2).

3. Results

3.1. Segmentation accuracy

Table 2 lists the AP50 and AP75 for whole-cell and nucleus segmentation. Cyto R-CNN achieves the highest accuracy for whole-cell segmentation, both in AP50 (58.65%) and AP75 (11.56%). For nucleus segmentation, Cyto R-CNN achieves the highest AP50 (78.32%) and StarDist the highest AP75 (47.24%). QuPath and Cellpose are being outperformed in all categories.

For additional context, we also provide the average precision that would arise from performing cell expansion on a perfect nucleus ground-truth. The results of this experiment are stated in the last row of Table 2. This theoretical setup achieved a whole cell AP50 of 56.22% and an AP75 of 1.07%.

Table 1
Test statistics D of the Kolmogorov–Smirnov test between each model and the gold standard.

Feature	Deeplabv3+	QuPath Default	QuPath Finetuned	StarDist	Cellpose	Cyto R-CNN
Area	0.26	0.54	0.26	0.32	0.27	0.25
Perimeter	0.36	0.60	0.42	0.49	0.40	0.29
Circularity	0.50	0.31	0.61	0.61	0.47	0.24
Solidity	0.49	0.11	0.48	0.55	0.46	0.24
Max. diameter	0.22	0.64	0.48	0.56	0.42	0.34
Min. diameter	0.31	0.39	0.17	0.21	0.19	0.20
Nucleus-to-Cell Ratio	0.35	0.17	0.37	0.41	0.51	0.17
Hematoxylin Median	0.28	0.11	0.24	0.13	0.19	0.14
Hematoxylin Mean	0.30	0.10	0.17	0.13	0.19	0.11
Hematoxylin Std. Dev.	0.27	0.05	0.17	0.12	0.05	0.07
Hematoxylin Max.	0.29	0.17	0.09	0.05	0.07	0.03
Hematoxylin Min.	0.11	0.13	0.13	0.10	0.19	0.04
Eosin Median	0.45	0.10	0.16	0.15	0.19	0.13
Eosin Mean	0.45	0.07	0.17	0.15	0.14	0.11
Eosin Std. Dev.	0.37	0.06	0.17	0.12	0.10	0.08
Eosin Max.	0.31	0.07	0.06	0.06	0.07	0.07
Eosin Min.	0.37	0.11	0.11	0.08	0.08	0.05

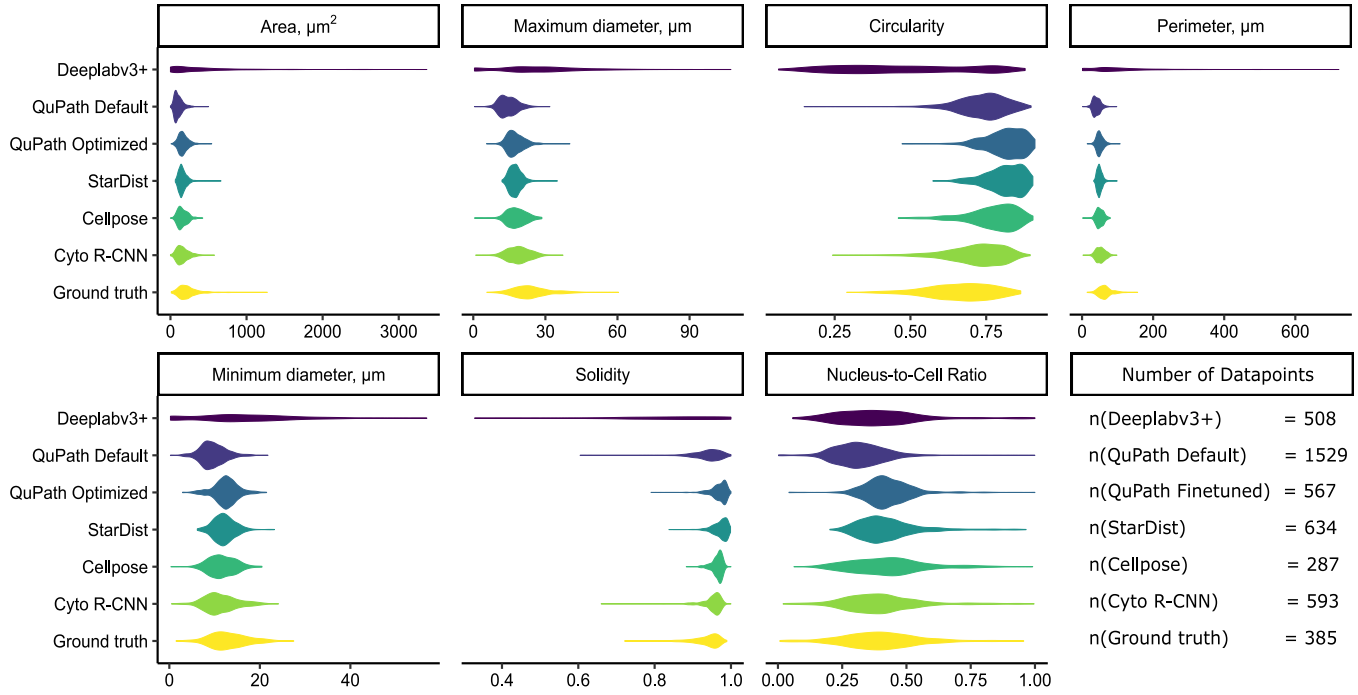

Fig. 3. Measurements of morphological whole-cell features as obtained via different segmentation methods. The measurements have been obtained by first converting segmentation masks into GeoJSON files, importing them into QuPath and then using built-in functionalities to calculate shape and staining features.

3.2. Measurement of cell features

The cell measurements as calculated by QuPath are visualized in Figs. 3 and 4. A tabular representation of these values can be found in the supplementary material.

The test statistic D of the Kolmogorov–Smirnov test (cf. Table 1) provides a quantification of how similar the distribution of predicted cell features are to the distribution of the gold standard. D ranges from 0 (perfect resemblance to the gold standard) to 1 (strong deviation from the gold standard). The cell area and perimeter were best approximated by Cyto R-CNN ($D_{area} = 0.25$, $D_{perimeter} = 0.29$). StarDist, Cellpose, Deeplabv3+ and finetuned QuPath could offer comparable performance in some cases ($0.26 \leq D \leq 0.49$), while the default QuPath settings resulted in clearly different measurements ($D_{area} = 0.54$, $D_{perimeter} = 0.60$). Regarding the cell circularity, Cyto R-CNN was the most accurate method ($D = 0.24$), followed by QuPath's default ($D = 0.31$). Other methods were significantly worse ($0.46 \leq D \leq 0.61$). The cell solidity was best approximated by QuPath's default ($D = 0.11$). Cyto R-CNN offered the second best approximation ($D = 0.24$). For the maximum diameter, the best results were obtained by Deeplabv3+ ($D = 0.22$),

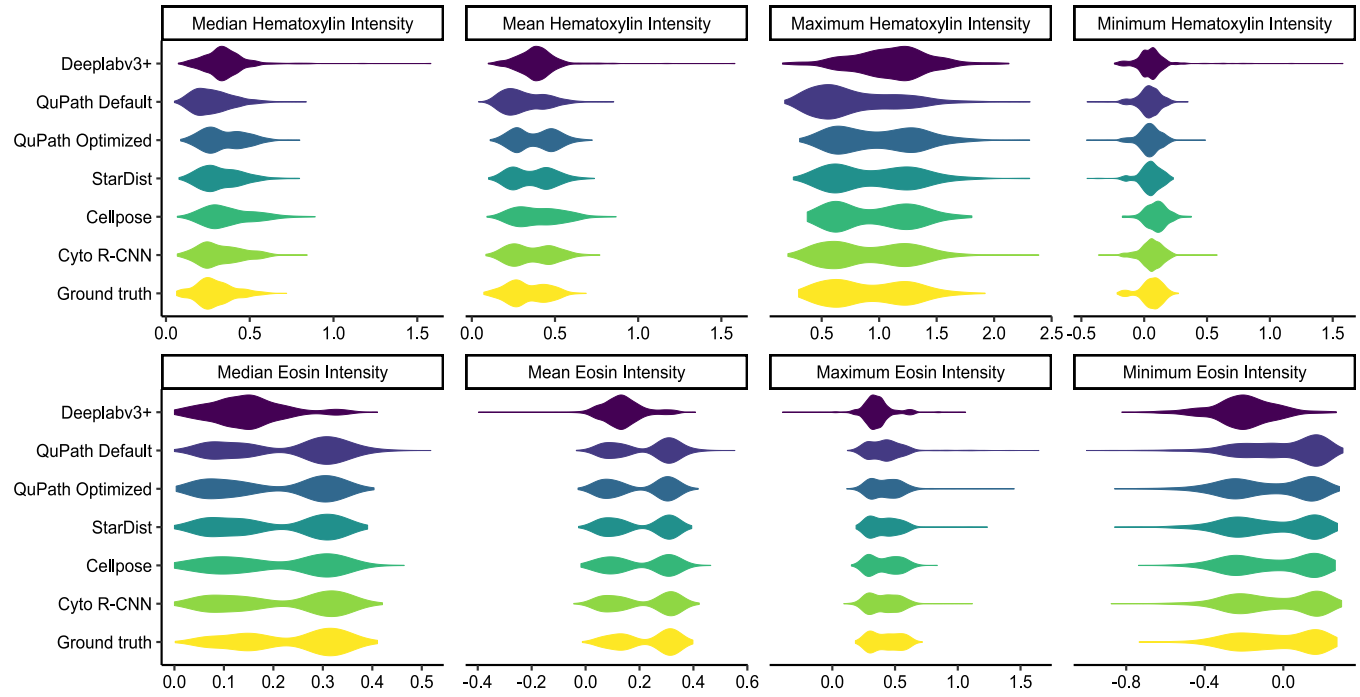

Fig. 4. Measurements of whole-cell staining features resulting from different segmentation methods. The above measurements have been obtained by first converting segmentation masks into GeoJSON files, importing them into QuPath and then using built-in functionalities to calculate shape and staining features.

Table 2
Average precision of different algorithms on the test dataset.

Model	AP50 nucleus	AP75 nucleus	AP50 cell	AP75 cell
Deeplabv3+	37.58%	9.23%	3.97%	1.01%
QuPath Default	22.95%	6.85%	11.12%	0.28%
QuPath Finetuned	35.24%	11.07%	19.46%	0.91%
Cellpose	48.35%	23.84%	31.85%	5.61%
StarDist	70.36%	**47.24%**	45.33%	2.32%
Cyto R-CNN	**78.32%**	42.54%	**58.65%**	**11.56%**
Perfect nucleus with cell expansion	–	–	56.22%	1.07%

followed by Cyto R-CNN ($D = 0.34$) and Cellpose ($D = 0.42$). The minimum diameter was best approximated by finetuned QuPath ($D = 0.17$), closely followed by Cellpose ($D = 0.19$), Cyto R-CNN ($D = 0.20$) and StarDist ($D = 0.21$). Deeplabv3+ and default QuPath was significantly worse in their performance ($D \geq 0.31$). For the nucleus-to-cell ratio, Cyto R-CNN and default QuPath offered the best performance ($D = 0.17$). All other methods were significantly worse ($0.35 \leq D \leq 0.51$). Hematoxylin median and mean intensity were best predicted by default QuPath ($D_{median} = 0.11$, $D_{mean} = 0.10$). However, all models offered similarly good performance ($0.10 \leq D \leq 0.28$). The cells' standard deviation of hematoxylin intensity was best approximated by default QuPath and Cellpose (both $D = 0.05$) with Cyto R-CNN following closely ($D = 0.07$). The best results for eosin median and mean intensity were delivered by QuPath Default ($D_{median} = 0.10$, $D_{mean} = 0.07$) and Cyto R-CNN ($D_{median} = 0.13$, $D_{mean} = 0.11$). The same applies to the standard deviation of eosin intensity ($D_{qupath} = 0.06$ and $D_{cytorcnn} = 0.08$). Minimum and maximum intensities of both hematoxylin and eosin were best approximated by Cyto R-CNN. Most other methods were generally close in performance ($0.03 \leq D \leq 0.17$). Only Deeplabv3+ showed large deviations from the ground truth ($D_{min} = 0.37$, $D_{max} = 0.31$).

Summarizing the results above, Cyto R-CNN's predictions show the highest similarity to the gold standard in 8 out of the 17 examined cell features. In 7 of the remaining 9 categories, Cyto R-CNN offers the second best approximation. In two categories, Cyto R-CNN provided third best results. Based on all 17 features Cyto R-CNN had the best average agreement with the ground truth ($\overline{D} = 0.15$) outperforming QuPath ($\overline{D} = 0.22$), StarDist ($\overline{D} = 0.25$) and Cellpose ($\overline{D} = 0.23$).

4. Discussion

The proposed architecture Cyto R-CNN enables segmentation of nucleus and cytoplasm in bright-field histological images. It outperforms QuPath, StarDist, Cellpose and a multi-scale Deeplabv3+ in whole-cell AP50 and AP75. Moreover, Cyto R-CNN's predictions are more reliable for measuring cell features than any other model.

These performance differences can be qualitatively explained by looking at a few example predictions in Fig. 5. The right-most column shows manual segmentations that are considered the gold standard. The first column from the left displays nuclei and cell masks as predicted by the multi-scale Deeplabv3+ model. As can be seen, the model clearly has difficulties separating individual objects in our dataset. Adjacent nuclei are often segmented as a single object. And boundaries of cell masks are often too large and overlapping each other. This is caused by to the underlying U-Net that produces a semantic segmentation mask only. The individual nuclei are only obtained by separating connected components. This heuristic can work well on cytological images, but does not produce good results on our histological dataset, where nuclei can be very close to each other. As a consequence, the scaled region proposals will fail to accurately capture single cells together with their cytoplasm. And as a result, the whole-cell segmentation masks will become inaccurate as well. The second column contains results from finetuned QuPath. Two things can be noticed: First, not all nuclei are detected. Second, the cytoplasm shape is very uniform. This is a direct result of nucleus expansion: When expanding a given shape outwards by a fixed number of pixels, the resulting shape will appear more circular. Differences in the original shape's curvature will be smoothed out. This leads to all cells appearing somewhat similar. The third column shows results of StarDist. The nuclei segmentations are of high quality, but the whole-cell segmentations are very uniform and

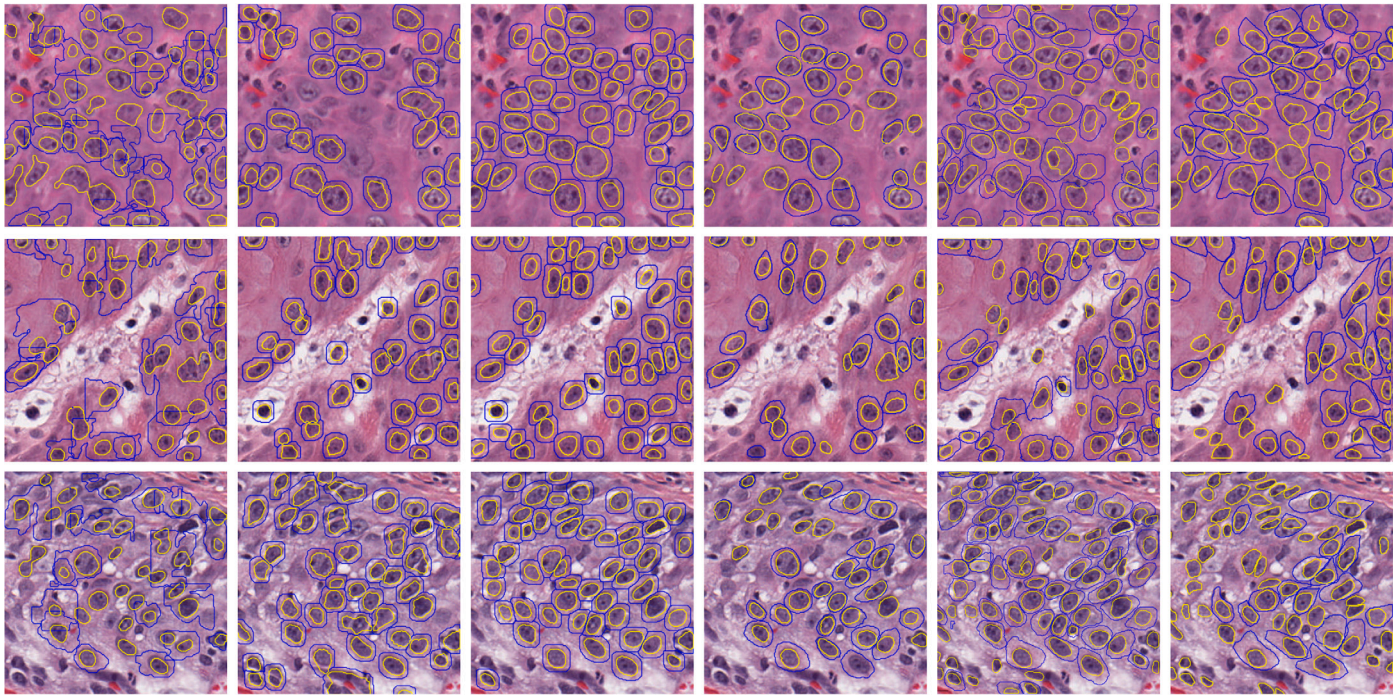

Fig. 5. Three images from the test dataset together with various nucleus and cell masks. Figures (a) to (e) show predicted object masks from different segmentation methods. Figure (f) displays the gold standard masks that were obtained through manual annotation. In figure (a) only some of the predicted masks from Deeplabv3+ are shown as the image would become too cluttered otherwise.

always resemble a circular shape. Just like with QuPath, this is the result of nucleus expansion. StarDist itself is a nucleus-only segmentation model. Combining it with nucleus expansion is popular in the literature [37,38], but does not yield good results in our experiments. The fourth column shows results of Cellpose. We can see that not all nuclei are detected, which is particularly visible in the third image. Apart from that, we see that nucleus and cytoplasm do not have a one-to-one correspondence. Many nuclei are without cytoplasm and some cytoplasm predictions do not have an underlying nucleus. This is a result of Cellpose's architecture, in which nucleus and cytoplasm are segmented by different models. This limitation of Cellpose does not seem to work well in our bright-field histological images. The fifth column shows the results of Cyto R-CNN. The nuclei segmentations are of high quality and the cytoplasm shapes are much more diverse. While there are a few cases of multi-nuclei cells and overlapping segmentations, Cyto R-CNN is the only model in this comparison that is able to segment non-trivial cell shapes.

4.1. Segmentation accuracy

Our segmentation results as reported in Table 2 meet expectations from the literature. The watershed algorithm is a traditional tool that has been surpassed by application-specific neural networks [39]. Thus, it is no surprise that QuPath performs worst in our experiments (AP50 22.95% with default parameters, AP50 35.24% with finetuned parameters). With such a low accuracy for the nucleus, it is expected that the cell segmentation as obtained by nucleus expansion is equally inaccurate (AP50 11.12% and 19.46%).

The Deeplabv3+ model is only slightly better than QuPath in terms of nucleus segmentation (AP50 47.58%). It segments nuclei with a regular U-Net that struggles with objects touching each other. Apart from that, its performance for whole-cell segmentation is very poor (AP50 3.97%). The Deeplabv3+ model seems to struggle with finding cell boundaries in our images. In contrast to the cytological images of SegPC-2021, the cell membrane in our dataset is much less pronounced, which can explain the learning difficulties.

Cellpose can already provide large improvements for both nucleus (AP50 48.35%) and cell segmentation (AP50 31.85%). However, Cellpose does not perform as well on our dataset as could be expected from its publication [21]. This is because our dataset only contains HE-stained images, for which Cellpose was not originally intended. The color contrast in HE is much lower than in immunohistological staining, so that the gradient tracking algorithm of Cellpose cannot work as well. This was previously observed by [32,40], who also reported non-optimal results for Cellpose on their datasets.

StarDist (AP50 70.36%) and Cyto R-CNN (78.32%) are the leading methods for nucleus segmentation in our experiments. The review by Lagree et al. [39] shows that this is in line with expectations from the literature. In their review, the authors compare Mask R-CNN, watershed and several U-Net based architectures on the MoNuSeg dataset [41], which also contains HE images. Mask R-CNN achieves an AP50 of 78.59%, which is similar to our results of Cyto R-CNN (78.32%). The best U-Net architecture achieves an AP50 of 71.66%, which is comparable to the results of StarDist in our experiments (70.36%). Even though StarDist achieves great results in nucleus segmentation, combining it with nucleus expansion only results in suboptimal accuracy (AP50 45.33%, AP75 2.32%). Cyto R-CNN is able to significantly outperform that both in AP50 (58.65%) and in AP75 (11.56%). It is important to note that Cyto R-CNN even outperforms the theoretical optimum of nucleus expansion. Our experiments show that even if a perfect nucleus segmentation is used as the input, the average precision (AP50 of 56.22% and AP75 of 1.07%) of cell expansion is surpassed by Cyto R-CNN.

Our results for whole-cell segmentation are comparable to the results of Jiang et al. [42]. In this paper, the authors develop a new method for whole-cell segmentation in cytological images and evaluate its performance on two different public datasets. In cytological images, the cell nucleus and cell membrane are much more pronounced than in our HE-stained images. However, cells are often overlapping, which

makes their task slightly different from ours. Nevertheless, the authors follow a similar approach for designing their architecture. They also extend Mask R-CNN by adding application-specific layers to it. Their new architecture achieves a mean average precision of 64.02% on one dataset and 49.43% on another. The results of our Cyto R-CNN (AP50 58.65%) are comparable to that. This shows that Mask R-CNN offers great potential for complex tasks such as whole-cell segmentation.

4.2. Dataset

To the authors' knowledge, CytoNuke is the first publicly available dataset of HE stained images which includes annotations for both the nucleus and the cytoplasm. Popular datasets such as PanNuke [43] and MoNuSeg [41] are limited to nuclei only. At the same time, they contain a number of different cell types (tumor, inflammatory, stromal cells) each of which have different cytoplasm characteristics. For some cells, the cytoplasm might not be visible at all or almost indistinguishable from the nucleus. This is often the case for lymphocytes for example. For this reason, it is not easily possible to extend existing datasets with whole-cell annotations. Thus, we decided to create our own quality-controlled dataset.

We intentionally limited it to one specific tumor cell type. HNSCC was chosen for multiple reasons. First, its similarity to regular epithelium allows for a clear visual distinction of the cell membrane [44]. Second, its cancer cells are known to be morphologically heterogeneous [45,46], making whole-cell segmentation a challenging task. Third, there are multiple hypotheses around morphological–clinical relations in HNSCC that could benefit from accurate segmentation methods [47–51]. With 6598 annotations (3991 nuclei and 2607 whole-cell), the size of our dataset is appropriate for a task as specific as whole-cell segmentation in bright-field histology. For reference, the PanNuke dataset contains around 3000 nuclei annotations for HNSCC.

4.3. Clinical impact

There is a huge potential for extracting clinically important information from cellular measurements in bright-field whole slide images. For example, it has been shown that the PDL-1 score of non-small cell lung carcinoma can be accurately predicted using only HE-staining [51]. And it was even found that certain nucleus shapes are associated with improved survival rates in HNSCC [52].

In absence of better methods, several papers make use of watershed, nucleus expansion and standard settings in QuPath. For example, Chen et al. [38] used nucleus expansion in 2022 to analyze macrophages in Covid-19. Bouhaddou et al. [37] used nucleus expansion to determine the presence of biomarkers in a cell. And Sadeghirad et al. [53] used it in 2023 to study the tumor microenvironment of HNSCC. Using nucleus expansion in these cases can be problematic. As we have shown in this paper, nucleus expansion is generally not a reliable method to obtain cell segmentations.

Based on our results, we can derive the following recommendations for clinical analyses of cell segmentations in HE images: First, one should use a more sophisticated method than watershed. Neural networks such as Cellpose, StarDist and Cyto R-CNN all offer better performance. The precise choice will depend on the application and should be validated before-hand. Second, one should be careful when using cell expansion. There might be cases in which it can be appropriately used. But without prior knowledge about the cell, one should not assume a circular cell shape, which will result from nucleus expansion.

4.4. Limitations and future work

Despite these promising results, there are some clear limitations of our study. Most importantly, we have limited ourselves to a small dataset of one particular cell type. HNSCC was a great starting point for developing our method because of the clearly visible cell cytoplasm and heterogeneous morphology. It remains to be shown if the results of Cyto R-CNN can be replicated on larger datasets of different cell types. There is also some potential to further improve the Cyto R-CNN architecture in the future. The cell scaling factor as described in Section 2.3.1 was set to a constant value that worked well for our dataset. When Cyto R-CNN will be applied to different cell types, it might be necessary to tune this scaling factor to a more appropriate values. Similarly, it could be possible to use multiple scaling factors simultaneously and train a new part of the network to rank the different proposals. A similar multi-scale approach is already known from cytological cell segmentation and proved successful in the SegPC-2021 challenge [25].

Apart from these possible improvements of Cyto R-CNN itself, there is now plenty of opportunity to develop completely new solutions for whole-cell segmentation using our newly created CytoNuke dataset. It would be interesting to investigate in the future whether more recent network architectures such as Mask2Former [54] can also be used for whole-cell segmentation. To achieve this, one would need to investigate to what extent geometric constraints (nucleus has to be inside the cytoplasm, maximum one cytoplasm per nucleus) can be translated at an architectural level.

Another interesting research area will be to modify existing cell segmentation methods from cytology in such a way that they can be successfully applied to HE-stained histological images. The SegPC-2021 challenge gave rise to several new cell segmentation methods that are promising candidates for future research. For example, Faura et al. [24] achieved the first place in the SegPC challenge and outperformed Deeplabv3+. However, this model operates under the assumption that each nucleus has a corresponding cytoplasm annotation. This assumption does not hold on our dataset. It would require some modifications to be able to apply the first-place solution to our dataset. This is why we settled with the second-place Deeplabv3+ for benchmarking purposes in this paper. Additionally, Salvi et al. [55] recently published a new architecture cyto-Knet that achieves even better results on the SegPC dataset. Its pre-processing and post-processing steps are quite specific for cytological images (e.g. allowing only a limited nuclei-to-cell ratio), but it will be interesting to examine in the future how well this method generalizes on histological images. We have made our CytoNuke dataset publicly available and are looking forward to seeing further progress in this area.

5. Conclusion

In this study, we developed a new method to accurately segment the whole cell together with its nucleus in bright-field histological images. This method has been able to outperform all alternatives, including the popular setup of combining StarDist with nucleus expansion. Moreover, we found that existing methods can result in misleading data for cell measurements and should not be used for cytometric analysis without further validation. Our new method is able to improve the reliability of such morphological measurements, which could be used for future studies.

Funding

Behrus Puladi was funded by the Medical Faculty of RWTH Aachen University as part of the Clinician Scientist Program. We acknowledge FWF enFaced 2.0 [KLI 1044, https://enfaced2.ikim.nrw/] and KITE (Plattform für KI-Translation Essen) from the REACT-EU initiative [https://kite.ikim.nrw/, EFRE-0801977]. Fabian Hörst, Jianning Li, Jens Kleesiek and Jan Egger received funding from the Cancer Research Center Cologne Essen (CCCE).

Institutional review board statement

All experiments have been approved by the ethics commission of RWTH Aachen University under the project number EK 486/20.

Code availability statement

The Cyto R-CNN code can be downloaded from https://github.com/OMFSdigital/Cyto-R-CNN.

CRediT authorship contribution statement

Johannes Raufeisen: Writing – review & editing, Writing – original draft, Visualization, Validation, Software, Methodology, Investigation, Formal analysis, Data curation, Conceptualization. **Kunpeng Xie:** Writing – review & editing, Validation, Data curation. **Fabian Hörst:** Writing – review & editing, Formal analysis. **Till Braunschweig:** Writing – review & editing, Validation. **Jianning Li:** Writing – review & editing, Formal analysis. **Jens Kleesiek:** Writing – review & editing, Methodology. **Rainer Röhrig:** Writing – review & editing, Formal analysis. **Jan Egger:** Writing – review & editing, Methodology, Formal analysis. **Bastian Leibe:** Writing – review & editing, Supervision, Resources. **Frank Hölzle:** Writing – review & editing, Supervision, Resources. **Alexander Hermans:** Writing – review & editing, Supervision, Methodology, Conceptualization. **Behrus Puladi:** Writing – review & editing, Visualization, Validation, Supervision, Resources, Project administration, Methodology, Investigation, Funding acquisition, Formal analysis, Data curation, Conceptualization.

Declaration of competing interest

The authors declare that they have no known competing financial interests or personal relationships that could have appeared to influence the work reported in this paper.

Data availability

The self-developed data set can be downloaded from Zenodo.org (https://doi.org/10.5281/zenodo.10560728) under CC-BY 4.0.

Acknowledgments

Data used in this publication were generated by the National Cancer Institute Clinical Proteomic Tumor Analysis Consortium (CPTAC). Simulations were performed with computing resources granted by RWTH Aachen University under project rwth1193.

Appendix A. Supplementary data

Supplementary material related to this article can be found online at https://doi.org/10.1016/j.cmpb.2024.108215.

References

[1] K.H. Yu, C. Zhang, G.J. Berry, R.B. Altman, C. Re, D.L. Rubin, M. Snyder, Predicting non-small cell lung cancer prognosis by fully automated microscopic pathology image features, Nature Commun. 7 (12474) (2016) http://dx.doi.org/10.1038/ncomms12474.

[2] J.N. Kather, A.T. Pearson, N. Halama, D. Jager, J. Krause, S.H. Loosen, A. Marx, P. Boor, F. Tacke, U.P. Neumann, H.I. Grabsch, T. Yoshikawa, H. Brenner, J. Chang-Claude, M. Hoffmeister, C. Trautwein, T. Luedde, Deep learning can predict microsatellite instability directly from histology in gastrointestinal cancer, Nat. Med. 25 (2019) 1054–1056, http://dx.doi.org/10.1038/s41591-019-0462-y.

[3] J.K. Chan, The wonderful colors of the hematoxylin-eosin stain in diagnostic surgical pathology, Int. J. Surg. Pathol. 22 (2014) 12–32, http://dx.doi.org/10.1177/1066896913517939.

[4] S.P. Border, P. Sarder, From what to why, the growing need for a focus shift toward explainability of ai in digital pathology, Front. Physiol. 12 (2021) 821217, http://dx.doi.org/10.3389/fphys.2021.821217.

[5] J.A. Diao, J.K. Wang, W.F. Chui, V. Mountain, S.C. Gullapally, R. Srinivasan, R.N. Mitchell, B. Glass, S. Hoffman, S.K. Rao, C. Maheshwari, A. Lahiri, A. Prakash, R. McLoughlin, J.K. Kerner, M.B. Resnick, M.C. Montalto, A. Khosla, I.N. Wapinski, A.H. Beck, H.L. Elliott, A. Taylor-Weiner, Human-interpretable image features derived from densely mapped cancer pathology slides predict diverse molecular phenotypes, Nature Commun. 12 (2021) 1613, http://dx.doi.org/10.1038/s41467-021-21896-9.

[6] H. Jiang, Y. Zhou, Y. Lin, R.C.K. Chan, J. Liu, H. Chen, Deep learning for computational cytology: A survey, Med. Image Anal. 84 (2023) 102691, http://dx.doi.org/10.1016/j.media.2022.102691.

[7] A. Gupta, S. Gehlot, S. Goswami, S. Motwani, R. Gupta, A.G. Faura, D. Stepec, T. Martincic, R. Azad, D. Merhof, A. Bozorgpour, B. Azad, A. Sulaiman, D. Pandey, P. Gupta, S. Bhattacharya, A. Sinha, R. Agarwal, X. Qiu, Y. Zhang, M. Fan, Y. Park, D. Lee, J.S. Park, K. Lee, J. Ye, Segpc-2021: A challenge & dataset on segmentation of multiple myeloma plasma cells from microscopic images, Med. Image Anal. 83 (2023) 102677, http://dx.doi.org/10.1016/j.media.2022.102677.

[8] P. Bankhead, M.B. Loughrey, J.A. Fernandez, Y. Dombrowski, D.G. McArt, P.D. Dunne, S. McQuaid, R.T. Gray, L.J. Murray, H.G. Coleman, J.A. James, M. Salto-Tellez, P.W. Hamilton, Qupath: Open source software for digital pathology image analysis, Sci. Rep. 7 (2017) 16878, http://dx.doi.org/10.1038/s41598-017-17204-5.

[9] U. Schmidt, M. Weigert, C. Broaddus, G. Myers, Cell detection with star-convex polygons, in: Medical Image Computing and Computer Assisted Intervention - Miccai 2018, Pt Ii 11071, 2018, pp. 265–273, http://dx.doi.org/10.1007/978-3-030-00934-2_30.

[10] A.E. Carpenter, T.R. Jones, M.R. Lamprecht, C. Clarke, I.H. Kang, O. Friman, D.A. Guertin, J.H. Chang, R.A. Lindquist, J. Moffat, P. Golland, D.M. Sabatini, Cellprofiler: image analysis software for identifying and quantifying cell phenotypes, Genome Biol. 7 (2006) R100, http://dx.doi.org/10.1186/gb-2006-7-10-r100.

[11] A.H. Scheel, H. Lamberty, Y. Tolkach, F. Gebauer, B. Schoemig-Markiefka, T. Zander, R. Buettner, J. Rueschoff, C.J. Bruns, W. Schroeder, A. Quaas, Tumour area infiltration and cell count in endoscopic biopsies of therapy-naive upper gi tract carcinomas by qupath analysis: implications for predictive biomarker testing, Sci. Rep. 13 (2023) 17580, http://dx.doi.org/10.1038/s41598-023-43903-3.

[12] A. Rodrigues, C. Nogueira, L.C. Marinho, G. Velozo, J. Sousa, P.G. Silva, F. Tavora, Computer-assisted tumor grading, validation of pd-l1 scoring, and quantification of cd8-positive immune cell density in urothelial carcinoma, a visual guide for pathologists using qupath, Surg. Exp. Pathol. 5 (2022) http://dx.doi.org/10.1186/s42047-022-00112-y.

[13] L. Berben, H. Wildiers, L. Marcelis, A. Antoranz, F. Bosisio, S. Hatse, G. Floris, Computerised scoring protocol for identification and quantification of different immune cell populations in breast tumour regions by the use of qupath software, Histopathology 77 (2020) 79–91, http://dx.doi.org/10.1111/his.14108.

[14] Y. Bai, K. Cole, S. Martinez-Morilla, F.S. Ahmed, J. Zugazagoitia, J. Staaf, A. Bosch, A. Ehinger, E. Nimeus, J. Hartman, B. Acs, D.L. Rimm, An open-source, automated tumor-infiltrating lymphocyte algorithm for prognosis in triple-negative breast cancer, Clin. Cancer Res. 27 (2021) 5557–5565, http://dx.doi.org/10.1158/1078-0432.CCR-21-0325.

[15] National Cancer Institute, Clinical proteomic tumor analysis consortium head and neck squamous cell carcinoma collection (cptac-hnscc) (version 14) [data set], in: The Cancer Imaging Archive, 2018, http://dx.doi.org/10.7937/K9/TCIA.2018.UW45NH81.

[16] K. Clark, B. Vendt, K. Smith, J. Freymann, J. Kirby, P. Koppel, S. Moore, S. Phillips, D. Maffitt, M. Pringle, L. Tarbox, F. Prior, The cancer imaging archive (tcia): Maintaining and operating a public information repository, J. Digit. Imaging 26 (2013) 1045–1057, http://dx.doi.org/10.1007/s10278-013-9622-7.

[17] M. Macenko, M. Niethammer, J.S. Marron, D. Borland, J.T. Woosley, X. Guan, C. Schmitt, N.E. Thomas, A method for normalizing histology slides for quantitative analysis, in: IEEE International Symposium on Biomedical Imaging: From Nano to Macro, IEEE, 2009, pp. 1107–1110, http://dx.doi.org/10.1109/isbi.2009.5193250.

[18] N. Kanwal, F. Perez-Bueno, A. Schmidt, K. Engan, R. Molina, The devil is in the details: Whole slide image acquisition and processing for artifacts detection, color variation, and data augmentation: A review, IEEE Access 10 (2022) 58821–58844, http://dx.doi.org/10.1109/access.2022.3176091.

[19] J.R. Kaczmarzyk, A. O'Callaghan, F. Inglis, S. Gat, T. Kurc, R. Gupta, E. Bremer, P. Bankhead, J.H. Saltz, Open and reusable deep learning for pathology with wsinfer and qupath, NPJ Precis. Oncol. 8 (2024) 9, http://dx.doi.org/10.1038/s41698-024-00499-9.

[20] L. Annaratone, M. Simonetti, E. Wernersson, C. Marchio, S. Garnerone, M.S. Scalzo, M. Bienko, R. Chiarle, A. Sapino, N. Crosetto, Quantification of her2 and estrogen receptor heterogeneity in breast cancer by single-molecule rna fluorescence in situ hybridization, Oncotarget 8 (2017) 18680–18698, http://dx.doi.org/10.18632/oncotarget.15727.

[21] C. Stringer, T. Wang, M. Michaelos, M. Pachitariu, Cellpose: A generalist algorithm for cellular segmentation, Nature Methods 18 (2021) 100–106, http://dx.doi.org/10.1038/s41592-020-01018-x.

[22] M. Reinbigler, J. Cosette, Z. Guesmia, S. Jimenez, C. Fetita, E. Brunet, D. Stockholm, Artificial intelligence workflow quantifying muscle features on hematoxylin-eosin stained sections reveals dystrophic phenotype amelioration upon treatment, Sci. Rep. 12 (2022) 19913, http://dx.doi.org/10.1038/s41598-022-24139-z.

[23] C. Stringer, M. Pachitariu, Cellpose 2.0: how to train your own model, 2022, http://dx.doi.org/10.1101/2022.04.01.486764, bioRxiv, 2022.04.01.486764.

[24] A.G. Faura, D. Štepec, T. Martinčič, D. Skočaj, Segmentation of multiple myeloma plasma cells in microscopy images with noisy labels, 2021, http://dx.doi.org/10.48550/arXiv.2111.05125.

[25] B. Afshin, A. Reza, S. Eman, S. Alaa, Multi-scale regional attention deeplab3+: multiple myeloma plasma cells segmentation in microscopic images, 2021, https://proceedings.mlr.press/v156/afshin21a.html.

[26] K.M. He, G. Gkioxari, P. Dollar, R. Girshick, Mask r-cnn, in: 2017 Ieee International Conference on Computer Vision, (Iccv), 2017, pp. 2980–2988, http://dx.doi.org/10.1109/Iccv.2017.322.

[27] L. Rettenberger, F. Rieken Münke, R. Bruch, M. Reischl, Mask r-cnn outperforms u-net in instance segmentation for overlapping cells, Curr. Dir. Biomed. Eng. 9 (2023) 335–338, http://dx.doi.org/10.1515/cdbme-2023-1084.

[28] G. Lv, K. Wen, Z. Wu, X. Jin, H. An, J. He, Nuclei r-cnn: Improve mask r-cnn for nuclei segmentation, in: 2019 IEEE 2nd International Conference on Information Communication and Signal Processing, (ICICSP), 2019, pp. 357–362, http://dx.doi.org/10.1109/ICICSP48821.2019.8958541.

[29] T.Y. Lin, M. Maire, S. Belongie, J. Hays, P. Perona, D. Ramanan, P. Dollár, C.L. Zitnick, Microsoft coco: Common objects in context, in: Computer Vision – ECCV 2014, Springer International Publishing, 2014, pp. 740–755, http://dx.doi.org/10.1007/978-3-319-10602-1_48.

[30] Y. Wu, A. Kirillov, F. Massa, W.Y. Lo, R. Girshick, Detectron2, 2019, https://github.com/facebookresearch/detectron2.

[31] Y. Han, Y. Lei, V. Shkolnikov, D. Xin, A. Auduong, S. Barcelo, J. Allebach, E.J. Delp, An ensemble method with edge awareness for abnormally shaped nuclei segmentation, in: Proceedings of the IEEE/CVF Conference on Computer Vision and Pattern Recognition, 2023, pp. 4314–4324, http://dx.doi.org/10.1109/CVPRW59228.2023.00454.

[32] Z. Lin, D. Wei, J. Lichtman, H. Pfister, Pytorch connectomics: A scalable and flexible segmentation framework for em connectomics, 2021, http://dx.doi.org/10.48550/arXiv.2112.05754, ArXiv.

[33] S.S. Al-Badran, L. Grant, M.V. Campo, J. Inthagard, K. Pennel, J. Quinn, P. Konanahalli, L. Hayman, P.G. Horgan, D.C. McMillan, C.S. Roxburgh, A. Roseweir, J.H. Park, J. Edwards, Relationship between immune checkpoint proteins, tumour microenvironment characteristics, and prognosis in primary operable colorectal cancer, J. Pathol. Clin. Res. 7 (2021) 121–134, http://dx.doi.org/10.1002/cjp2.193.

[34] J. Jiang, B. Tekin, R. Guo, H. Liu, Y. Huang, C. Wang, Digital pathology-based study of cell- and tissue-level morphologic features in serous borderline ovarian tumor and high-grade serous ovarian cancer, J. Pathol. Inform. 12 (24) (2021) http://dx.doi.org/10.4103/jpi.jpi_76_20.

[35] S. Lin, J.P. Samsoondar, E. Bandari, S. Keow, B. Bikash, D. Tan, J. Martinez-Acevedo, J. Loggie, M. Pham, N.J. Wu, T. Misra, V.H.K. Lam, I. Sansano, M.J. Cecchini, Digital quantification of tumor cellularity as a novel prognostic feature of non-small cell lung carcinoma, Mod. Pathol. 36 (2023) 100055, http://dx.doi.org/10.1016/j.modpat.2022.100055.

[36] W. Zhang, M.Y. Koh, D. Sirohi, J. Ying, B.J. Brintz, B.S. Knudsen, Predicting ihc staining classes of nf1 using features in the hematoxylin channel, J. Pathol. Inform. 14 (2023) 100196, http://dx.doi.org/10.1016/j.jpi.2023.100196.

[37] M. Bouhaddou, R.H. Lee, H. Li, N.E. Bhola, R.A. O'Keefe, M. Naser, T.R. Zhu, K. Nwachuku, U. Duvvuri, A.B. Olshen, R. Roy, A. Hechmer, J. Bolen, S.B. Keysar, A. Jimeno, G.B. Mills, S. Vandenberg, D.L. Swaney, D.E. Johnson, N.J. Krogan, J.R. Grandis, Caveolin-1 and sox-2 are predictive biomarkers of cetuximab response in head and neck cancer, JCI Insight 6 (2021) http://dx.doi.org/10.1172/jci.insight.151982.

[38] S.T. Chen, M.D. Park, D.M. Del Valle, M. Buckup, A. Tabachnikova, R.C. Thompson, N.W. Simons, K. Mouskas, B. Lee, D. Geanon, D. D'Souza, T. Dawson, R. Marvin, K. Nie, Z. Zhao, J. LeBerichel, C. Chang, H. Jamal, G. Akturk, U. Chaddha, K. Mathews, S. Acquah, S.A. Brown, M. Reiss, T. Harkin, M. Feldmann, C.A. Powell, J.L. Hook, S. Kim-Schulze, A.H. Rahman, B.D. Brown, C.B.T. Mount Sinai, N.D. Beckmann, S. Gnjatic, E. Kenigsberg, A.W. Charney, M. Merad, A shift in lung macrophage composition is associated with covid-19 severity and recovery, Sci. Transl. Med. 14 (2022) http://dx.doi.org/10.1126/scitranslmed.abn5168.

[39] A. Lagree, M. Mohebpour, N. Meti, K. Saednia, F.I. Lu, E. Slodkowska, S. Gandhi, E. Rakovitch, A. Shenfield, A. Sadeghi-Naini, W.T. Tran, A review and comparison of breast tumor cell nuclei segmentation performances using deep convolutional neural networks, Sci. Rep. 11 (2021) 8025, http://dx.doi.org/10.1038/s41598-021-87496-1.

[40] L. Lauenburg, Z. Lin, R. Zhang, M.D. Santos, S. Huang, I. Arganda-Carreras, E.S. Boyden, H. Pfister, D. Wei, 3D domain adaptive instance segmentation via cyclic segmentation gans, IEEE J. Biomed. Health Inform. 27 (2023) 4018–4027, http://dx.doi.org/10.1109/JBHI.2023.3281332.

[41] N. Kumar, R. Verma, S. Sharma, S. Bhargava, A. Vahadane, A. Sethi, A dataset and a technique for generalized nuclear segmentation for computational pathology, IEEE Trans. Med. Imaging 36 (2017) 1550–1560, http://dx.doi.org/10.1109/TMI.2017.2677499.

[42] H. Jiang, R. Zhang, Y. Zhou, Y. Wang, H. Chen, Donet: Deep de-overlapping network for cytology instance segmentation, in: Conference on Computer Vision and Pattern Recognition, (CVPR), pp. 15641–15650, http://dx.doi.org/10.48550/arXiv.2303.14373.

[43] J. Gamper, N. Alemi Koohbanani, K. Benet, A. Khuram, N. Rajpoot, Pannuke: An open pan-cancer histology dataset for nuclei instance segmentation and classification, in: European Congress on Digital Pathology, Springer, pp. 11–19, http://dx.doi.org/10.1007/978-3-030-23937-4_2.

[44] D.E. Johnson, B. Burtness, C.R. Leemans, V.W.Y. Lui, J.E. Bauman, J.R. Grandis, Head and neck squamous cell carcinoma, Nat. Rev. Dis. Primers 6 (2020) 92, http://dx.doi.org/10.1038/s41572-020-00224-3.

[45] A.D. Singhi, E.B. Stelow, S.E. Mills, W.H. Westra, Lymphoepithelial-like carcinoma of the oropharynx: A morphologic variant of hpv-related head and neck carcinoma, Am. J. Surg. Pathol. 34 (2010) 800–805, http://dx.doi.org/10.1097/PAS.0b013e3181d9ba21.

[46] W.H. Westra, The morphologic profile of hpv-related head and neck squamous carcinoma: implications for diagnosis, prognosis, and clinical management, Head Neck Pathol. 6 (Suppl 1) (2012) S48–54, http://dx.doi.org/10.1007/s12105-012-0371-6.

[47] R.K. Davis, C. Fox, D.K. Heffner, Computerized nuclear morphometry: A reproducible cytopathologic marker of head and neck cancer, Otolaryngol. Head Neck Surg. 96 (1987) 15–21, http://dx.doi.org/10.1177/019459988709600103.

[48] R.J. Briggs, K.J. Pienta, R.H. Hruban, W.J. Richtsmeier, Nuclear morphometry for prediction of metastatic potential in early squamous cell carcinoma of the floor of the mouth, Arch. Otolaryngol. Head Neck Surg. 118 (1992) 531–533, http://dx.doi.org/10.1001/archotol.1992.01880050085020.

[49] J. Sekine, M. Uehara, K. Hideshima, A. Irie, T. Inokuchi, Predictability of lymph node metastases by preoperative nuclear morphometry in squamous cell carcinoma of the tongue, Cancer Detect. Prev. 27 (2003) 427–433, http://dx.doi.org/10.1016/j.cdp.2003.09.001.

[50] B.M. Biswal, N.H. Othman, Correlation of nuclear morphometry and agnor score with radiation response in squamous cell cancers of the head and neck: A preliminary study, Malays. J. Med. Sci. 17 (2010) 19–26, https://www.ncbi.nlm.nih.gov/pmc/articles/PMC3216171/.

[51] J.R. Naso, T. Povshedna, G. Wang, N. Banyi, C. MacAulay, D.N. Ionescu, C. Zhou, Automated pd-l1 scoring for non-small cell lung carcinoma using open-source software, Pathol. Oncol. Res. 27 (2021) 609717, http://dx.doi.org/10.3389/pore.2021.609717.

[52] P. Bose, N.T. Brockton, K. Guggisberg, S.C. Nakoneshny, E. Kornaga, A.C. Klimowicz, M. Tambasco, J.C. Dort, Fractal analysis of nuclear histology integrates tumor and stromal features into a single prognostic factor of the oral cancer microenvironment, BMC Cancer 15 (2015) 409, http://dx.doi.org/10.1186/s12885-015-1380-0.

[53] H. Sadeghirad, N. Liu, J. Monkman, N. Ma, B.B. Cheikh, N. Jhaveri, C.W. Tan, M.E. Warkiani, M.N. Adams, Q. Nguyen, R. Ladwa, O. Braubach, K. O'Byrne, M. Davis, B.G.M. Hughes, A. Kulasinghe, Compartmentalized spatial profiling of the tumor microenvironment in head and neck squamous cell carcinoma identifies immune checkpoint molecules and tumor necrosis factor receptor superfamily members as biomarkers of response to immunotherapy, Front. Immunol. 14 (2023) 1135489, http://dx.doi.org/10.3389/fimmu.2023.1135489.

[54] B.C. Girdhar, I. Misra, A.G. Schwing, A. Kirillov, Rohit, Masked-attention mask transformer for universal image segmentation, 2022, http://dx.doi.org/10.48550/arXiv.2112.01527.

[55] M. Salvi, N. Michielli, K.M. Meiburger, C. Cattelino, B. Cotrufo, M. Giacosa, C. Giovanzana, F. Molinari, Cyto-knet: An instance segmentation approach for multiple myeloma plasma cells using conditional kernels, Int. J. Imaging Syst. Technol. 34 (2023) http://dx.doi.org/10.1002/ima.22984.